# Regulation of exosome secretion by Rab35 and its GTPase-activating proteins TBC1D10A–C

Chieh Hsu,[3] Yuichi Morohashi,[5] Shin-ichiro Yoshimura,[5] Natalia Manrique-Hoyos,[3] SangYong Jung,[2] Marcel A. Lauterbach,[7] Mostafa Bakhti,[3] Mads Grønborg,[6] Wiebke Möbius,[1] JeongSeop Rhee,[2] Francis A. Barr,[5] and Mikael Simons[3,4]

[1]Department of Neurogenetics and [2]Department of Molecular Neurobiology, [3]Max Planck Institute for Experimental Medicine, 37075 Göttingen, Germany
[4]Department of Neurology, University of Göttingen, 37075 Göttingen, Germany
[5]University of Liverpool Cancer Research Centre, Liverpool L3 9TA, England, UK
[6]Department of Neurobiology and [7]Department of NanoBiophotonics, Max Planck Institute for Biophysical Chemistry, 37077 Göttingen, Germany

Oligodendrocytes secrete vesicles into the extracellular space, where they might play a role in neuron–glia communication. These exosomes are small vesicles with a diameter of 50–100 nm that are formed within multivesicular bodies and are released after fusion with the plasma membrane. The intracellular pathways that generate exosomes are poorly defined. Because Rab family guanosine triphosphatases (GTPases) together with their regulators are important membrane trafficking organizers, we investigated which Rab GTPase-activating proteins interfere with exosome release. We find that TBC1D10A–C regulate exosome secretion in a catalytic activity–dependent manner. We show that Rab35 is the target of TBC1D10A–C and that the inhibition of Rab35 function leads to intracellular accumulation of endosomal vesicles and impairs exosome secretion. Rab35 localizes to the surface of oligodendroglia in a GTP-dependent manner, where it increases the density of vesicles, suggesting a function in docking or tethering. These findings provide a basis for understanding the biogenesis and function of exosomes in the central nervous system.

## Introduction

After endocytosis, proteins and lipids that are destined for lysosomal degradation are first incorporated into intraluminal vesicles of multivesicular bodies (MVBs) and are then delivered to lysosomes for degradation (Gruenberg and Stenmark, 2004; Piper and Katzmann, 2007). Alternatively, MVBs can directly fuse with the plasma membrane, leading to release of the intraluminal vesicles into the extracellular environment as exosomes, where they play an important role in processes such as protein turnover, intercellular signaling, transfer of mRNA, angiogenesis, and tumor spreading (Lakkaraju and Rodriguez-Boulan, 2008; Schorey and Bhatnagar, 2008; Buschow et al., 2009; Korkut et al., 2009; Simons and Raposo, 2009; Théry et al., 2009).

How proteins and lipids are sorted to these subsets of MVBs directed either for lysosomal degradation or for secretion as exosomes is presently unknown. Because the Rab family GTPase proteins show a characteristic subcellular distribution and represent an important determinant of organelle identity (Stenmark, 2009), we address herein the question of cargo separation by studying the role of Rab proteins in exosome release in oligodendroglial cells.

Although previous work has shown that the subsequent activity of Rab5 and -7 is required to transport cargo through the endosomal system to lysosomes to mediate its degradation (Stenmark, 2009), much less is known about Rabs required for delivery of exosomal cargo. To address this issue, we used Oli-neu cells, an oligodendroglial cell line that contains a large number of MVBs and secretes substantial amounts of exosomes as a model system. In these cells, the proteolipid protein (PLP), the major protein of myelin of the central nervous system, is localized to a large extent in MVBs, from where it can be transported back to the plasma membrane to be secreted in association

Correspondence to Mikael Simons: msimons@gwdg.de

Abbreviations used in this paper: GAP, GTPase-activating protein; GFAP, glial fibrillary acidic protein; LC, liquid chromatography; MS, mass spectrometry; MVB, multivesicular body; NP, nitrophenyl; PLP, proteolipid protein; RRP, readily releasable pool; TIRF, total internal reflection fluorescence.



The Rockefeller University Press $30.00
J. Cell Biol. Vol. 189 No. 2 223–232
www.jcb.org/cgi/doi/10.1083/jcb.200911018

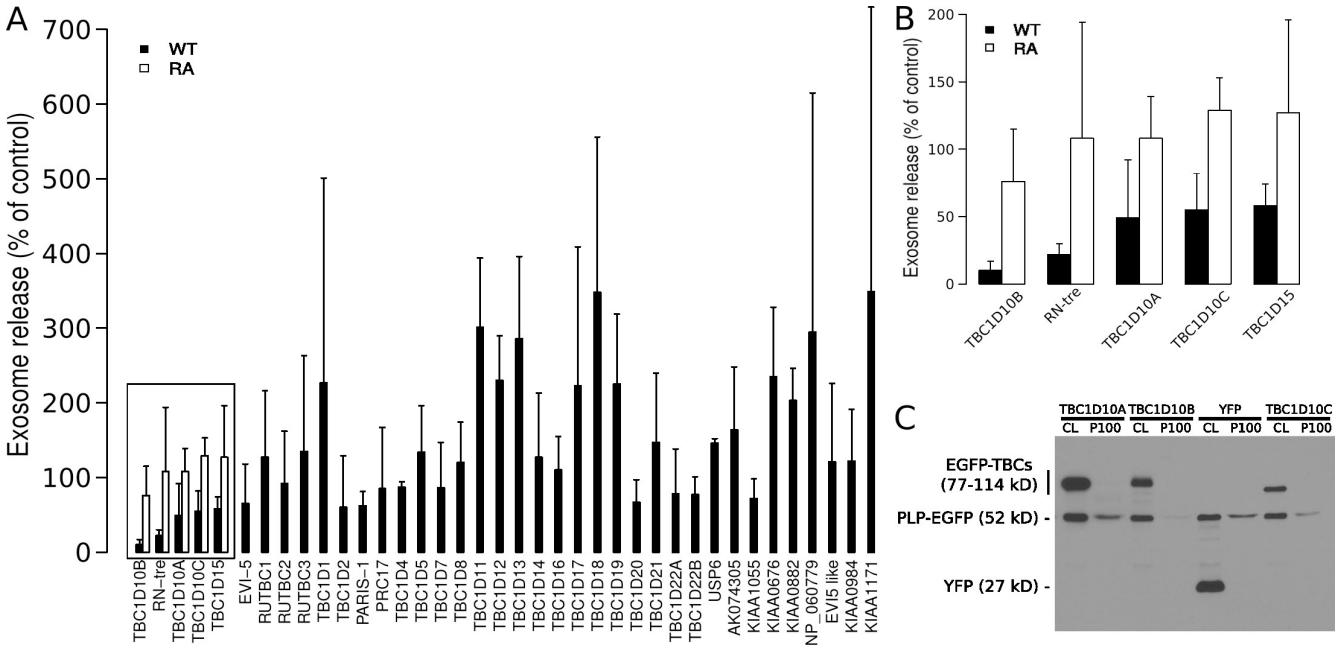


Figure 1. **Screen of a Rab GAP library identifies the TBC1D10 family as regulators of exosome secretion.** (A and B) PLP-EGFP was coexpressed with a library of 38 different EGFP-tagged wild-type (WT) Rab GAPs in Oli-neu cells using a plasmid ratio of 2:1 (EGFP-TBC/PLP-EGFP). Cells transfected with both PLP-EFP and YFP were used as a reference. 16 h after transfections, the cells were switched to serum-free medium, and the medium was collected after ~4 h of further incubation before submitting it to sequential centrifugation steps. The resulting 100,000 *g* pellets (exosome fraction) of each centrifugation step were analyzed by Western blotting for PLP-EGFP and the EGFP-TBCs (Rab GAPs) by anti-GFP antibodies. The mean of three independent experiments is shown in the graph. Those Rab GAPs that reduced exosome release of PLP below 60% of the control (boxed), were compared with their catalytically inactive arginine to alanine (RA) mutants, and the zoomed-in graph is shown in B. Error bars indicate the SD. (C) Western blot of the cell lysates (CL) and 100,000 *g* pellets (P100) is shown for one representative experiment with TBC1D10.

with exosomes (Trajkovic et al., 2006, 2008; Krämer-Albers et al., 2007).

## Results and discussion

We started our screen for Rab GTPases in exosome secretion by performing a proteome analysis of purified exosomes using liquid chromatography (LC) coupled to tandem mass spectrometry (MS; LC-MS/MS). A total of 301 proteins were identified, of which approximately one third have been previously found in exosomes from other cell types (Barile et al., 2005; Segura et al., 2005; Aoki et al., 2007; Valadi et al., 2007; Conde-Vancells et al., 2008), confirming the purity of the preparation. Among the identified proteins was a relatively large number of Rab GTPases (Rab1a, -1b, -2a, -5b, -5c, -6a, -7, -8b, -10, -11b, and -35), many of which have previously been implicated in endosomal membrane trafficking (Stenmark, 2009). To analyze the relative abundance of the Rab GTPases in exosomes, we expressed all of the identified Rabs as EGFP fusion proteins in Oli-neu cells and compared the levels with PLP. As compared with PLP-EGFP, Rab proteins were found at relatively low levels in exosomes, but among the most abundant was EGFP-Rab35 (Fig. S1 and Table S1).

To define the requirement of Rab proteins in exosome biogenesis, a Rab GTPase-activating protein (GAP) library was screened for the ability of each Rab GAP to reduce the secretion of PLP-EGFP in association with exosomes. Because Rab GAPs promote GTP hydrolysis of Rabs requiring a conserved catalytic domain, the TBC (Tre/Bub2/Cdc16) domain, this approach leads to the selective inactivation of the different Rab proteins (Fuchs et al., 2007; Yoshimura et al., 2007). We coexpressed PLP-EGFP with EGFP fusion proteins of all 38 predicted Rab GAPs, confirmed their expression by Western blotting with anti-GFP antibodies in the cell lysates, and determined the amount of PLP-EGFP in the exosomal membrane fraction in three independent experiments. We did not focus on the GAPs that seemed to enhance exosome secretion because an increase of membrane in the extracellular medium could also be caused by more cell debris as a result of cell toxicity. The positive candidates that reproducibly reduced the release of PLP-GFP with exosomes were reevaluated by comparing the effects of the wild-type GAPs with that of the catalytically inactive point mutations. We found that TBC1D10B, RN-tre, TBC1D10A, TBC1D10C, and TBC1D15 reduced PLP-EGFP recovery from the exosomal membrane fraction in a catalytic activity–dependent manner (Fig. 1). RN-tre has been reported to act on Rab5 (Lanzetti et al., 2000) and Rab43 (Haas et al., 2005), TBC1D15 on Rab7 (Zhang et al., 2005), TBC1D10A on Rab27a (Itoh and Fukuda, 2006), and TBC1D10C on Rab35 (Patino-Lopez et al., 2008). We reexamined the effects of the TBC1D10 family toward specific Rab proteins by testing their ability to accelerate GTP hydrolysis in a biochemical assay with a wide set of Rabs (Fig. 2). These data clearly show that all three members of the TBC1D10 family have strong and Rab35-specific GAP activity. TBC1D10B, which reduced exosome secretion most potently, showed the strongest activity toward

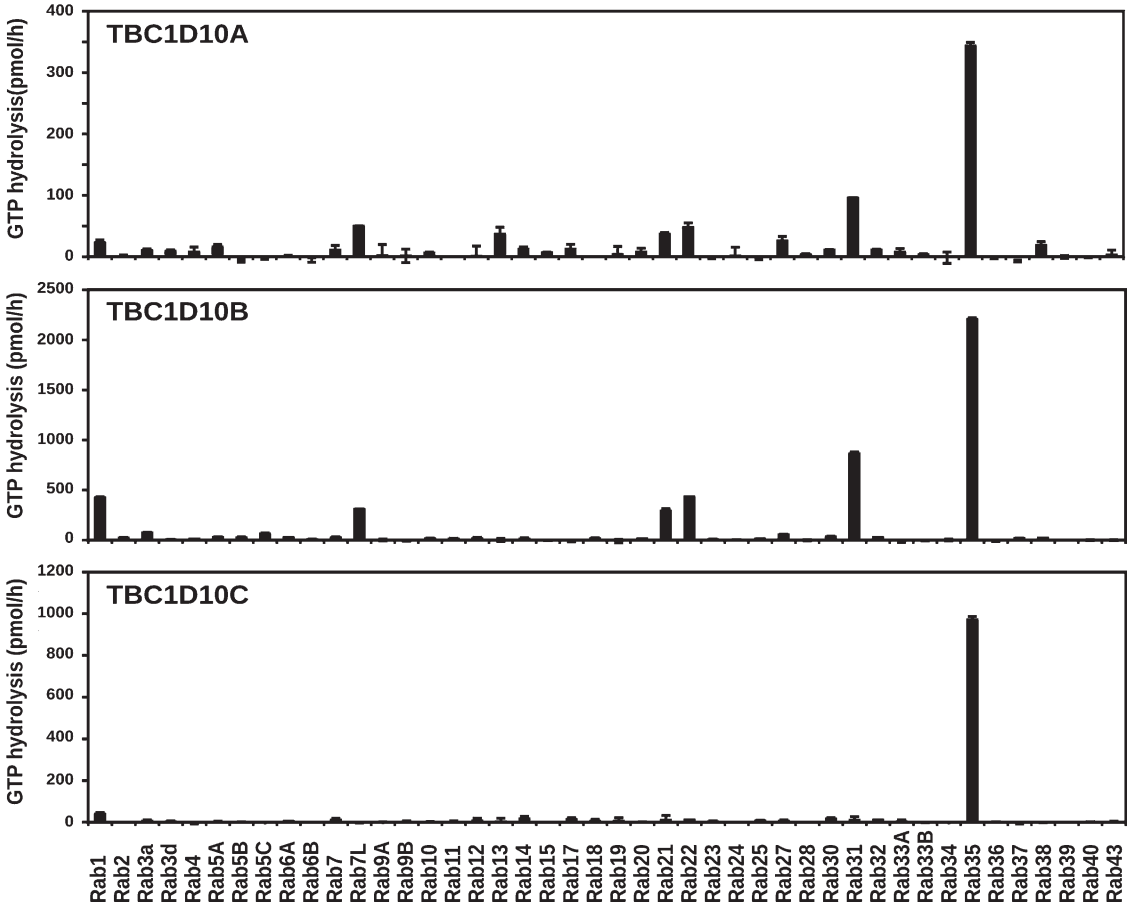


Figure 2. **Identification of Rab35 as the target of TBC1D10A–C.** Biochemical GAP assays were performed using recombinant hexahistidine-GST–tagged human Rab GTPases and hexahistidine-tagged TBC1D10 family proteins. Reactions were performed for 60 min at 37°C, using 100 pmol GST-Rab and 10 pmol hexahistidine-tagged TBC1D10A, -B, or -C. GTP hydrolysis is plotted in picomoles per hour. Error bars represent SD.

Rab35 (>2,000 pmol/h of hydrolyzed GTP; Fig. 2). We coexpressed the GTP-locked Rab35$^{Q67A}$ mutant, which is resistant to GAP activity, with TBC1D10B and observed an approximate twofold increase in exosome release of PLP (Fig. 3, A and B).

Because our results from the Rab GAP screen pointed to a possible role of Rab35 in the exosome pathway, we used the dominant-negative mutant of Rab35 (Rab35$^{N120I}$) to interfere with its function and found that it significantly decreased release of PLP with exosomes (Fig. 3, C and F). We continued the analysis of the function of Rab35 by performing RNAi knockdown experiments. Knockdown of Rab35 by two rounds of siRNA nucleofection efficiently depleted Rab35 from the cell lysate and resulted in a significant reduction of PLP recovery from the exosomal membrane fraction (Fig. 3, D–F), confirming the findings with the dominant-negative mutant. Relatively little is known about the function of Rab35 except of its role in receptor recycling, cytokinesis, and actin reorganization (Kouranti et al., 2006; Patino-Lopez et al., 2008; Sato et al., 2008; Walseng et al., 2008; Zhang et al., 2009).

To analyze where Rab35 may act in oligodendroglial cells, we analyzed the localization of EGFP-tagged Rab35 by confocal microscopy. Wild-type Rab35, the GTP-locked Rab35$^{Q67A}$, and its GAP, TBC1D10B, were detected at the plasma membrane, whereas the nucleotide-free Rab35$^{N120I}$ and the GDP-locked Rab35$^{S22N}$ were mainly found within the cytosol and in vesicles that contained PLP and Lamp-1, identifying them as late endosomes/lysosomes (Fig. 4, A and B). Similar findings were obtained when Rab35 and its mutant were expressed in HeLa cells, with the exception of more intracellular wild-type EGFP-Rab35 in vesicles containing PLP-myc (Fig. S2). We observed an expansion of the cell surface area after expression of either wild-type Rab35 or constitutively active GTP-locked Rab35$^{Q67A}$ (Fig. 4 A).

To obtain further evidence for the plasma membrane localization of Rab35, we analyzed the expression of Rab35 in myelin, a plasma membrane extension of oligodendrocytes which is formed during the development of the central nervous system by the spiral wrapping of glial membrane around the axons (Sherman and Brophy, 2005; Simons and Trotter, 2007; Barres, 2008). Indeed, we detected Rab35 at relatively high levels in the lysates of purified myelin by Western blotting (Fig. 4 D). Purified myelin did not contain glial fibrillary acidic protein (GFAP) or synaptophysin proteins specific to astrocytes and neurons, confirming the purity of isolated myelin (Fig. 4 E). Although the majority of myelin consists of tightly stacked membrane bilayers with no space for MVBs, a fraction of myelin is composed of more loosely organized membrane that contains larger cytoplasmic channels (e.g., paranodal

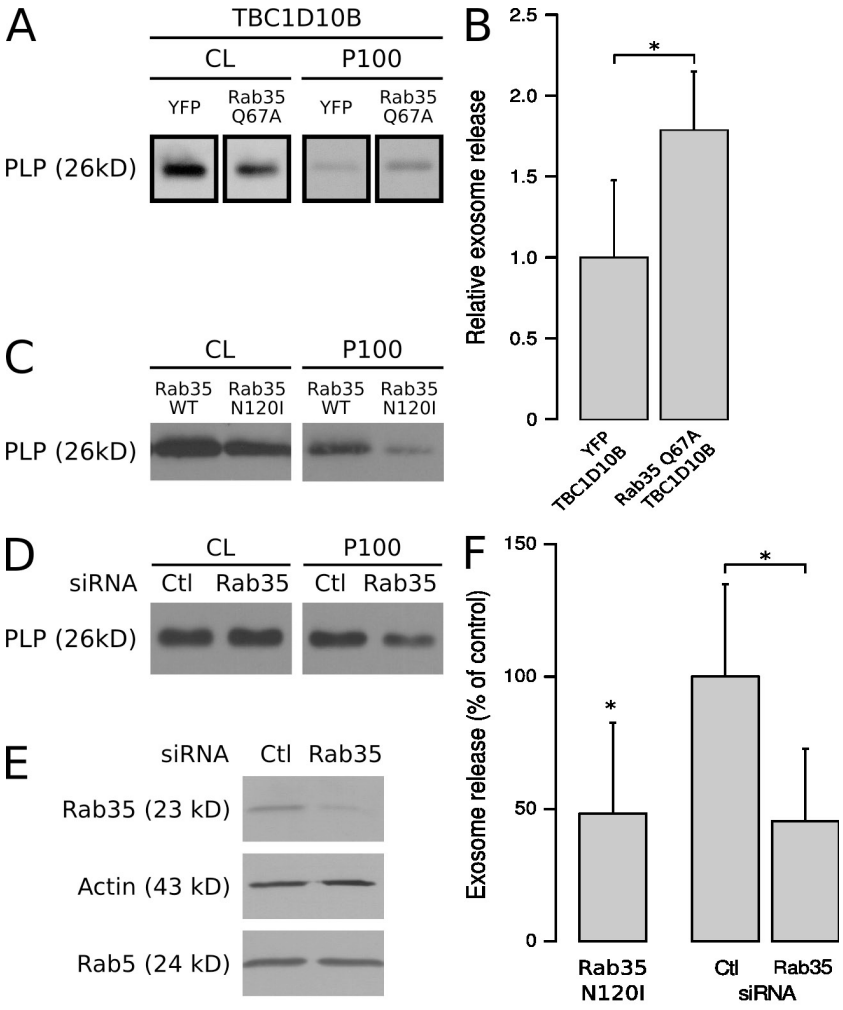


Figure 3. **Inhibition of Rab35 function reduces exosome secretion of PLP.** (A) Cells were transfected with PLP-myc, TBC1D10B, and either YFP or Rab35$^{Q67A}$. The amounts of PLP in the cell lysates (CL) and 100,000 *g* pellets (P100) were quantified, and the results of two experiments performed in duplicates are shown in B (values represent the mean ± SD; *, P < 0.05; Welch's two-sample *t* test). (C) Cells were transfected with PLP-myc together with either wild-type (WT) Rab35 or the dominant-negative mutant (Rab35$^{N120I}$). (D and E) After delivery of control (Ctl) or siRNA against Rab35 into cells by nucleofection, the cell lysates were analyzed by Western blotting with Rab35 antibodies to monitor knockdown efficiency. Actin and Rab5 were used as controls. The amount of PLP in the cell lysates and 100,000 *g* pellets were determined after Rab35 RNAi. (F) Results are expressed as the mean ± SD of four experiments (*, P < 0.05; one-sample *t* test and Welch's two-sample *t* test).

loops and abaxonal space; Salzer, 2003). We performed electron microscopy to analyze whether these structures contained MVBs. MVBs were frequently found in noncompacted regions of myelin (Fig. 4 F; Trapp et al., 1989), and immunoelectron microscopy revealed that MVBs contained PLP (Fig. 4 F). Because the Rab35 antibody did not work reliably in immunohistochemistry, we purified noncompacted myelin from crude myelin by sucrose gradient centrifugations to determine the localization of Rab35 in myelin. Rab35 was not found in the light fraction, which is enriched in compact myelin, but was recovered from the heavier fraction, which also contained contactin, a protein which localizes to the paranodal junction (Fig. 4 E; Rios et al., 2000).

To define the steps at which Rab35 might act, we compared the effects of the dominant-negative Rab7 and Rab35 mutants. We found that only the expression of Rab7$^{T22N}$ but not Rab35$^{N120I}$ or Rab35$^{S22N}$ resulted in an enlargement of PLP-containing, Lamp-1–positive organelles and increased the colocalization of PLP and Lamp-1 (Fig. 4, A and C; and Fig. S3). In addition, we only observed a reduction of EGF degradation after Rab7$^{T22N}$ but not after Rab35$^{N120I}$ expression (Fig. S3), suggesting that lysosomal degradation is not regulated by Rab35.

To determine how Rab35 functions, we performed RNAi experiments to deplete Rab35 and analyzed the number and size of the PLP-containing intracellular vesicles. Although vesicle size was unaffected, the total number of vesicles increased by ∼35% after Rab35 knockdown (Fig. 5, A–C). These vesicles were identified as late endosomes/lysosomes based on their colocalization with Lamp-1. The intracellular accumulation of PLP in Lamp-1–positive vesicles and the reduction in exosome secretion after Rab35 depletion suggests that a pathway from the endosomal system to the plasma membrane is regulated by Rab35.

To analyze the possibility that Rab35 controls vesicular movement, time-lapse experiments were performed using LysoTracker as a probe to identify PLP/Lamp-1–containing endosomes (85.6 ± 2.7% of the LysoTracker-labeled vesicles contained PLP-EGFP; $n$ = 1,522 vesicles analyzed). The effects of the constitutive active and inactive mutants of Rab35 were compared in their ability to influence the mobility of endosomes. We used a recently developed algorithm to indentify and track individual vesicles automatically in a video sequence (Westphal et al., 2008). Data from 47 videos from three independent experiments were pooled to provide a quantitative assessment of vesicle motility. Surprisingly, we found that active GTP-locked Rab35$^{Q67A}$ slightly reduced the motility of LysoTracker-labeled vesicles (by 14.6% ± 3.8% as compared with Rab35$^{S22N}$; $n$ = ∼1,800 vesicles; P < 0.001, Welch's

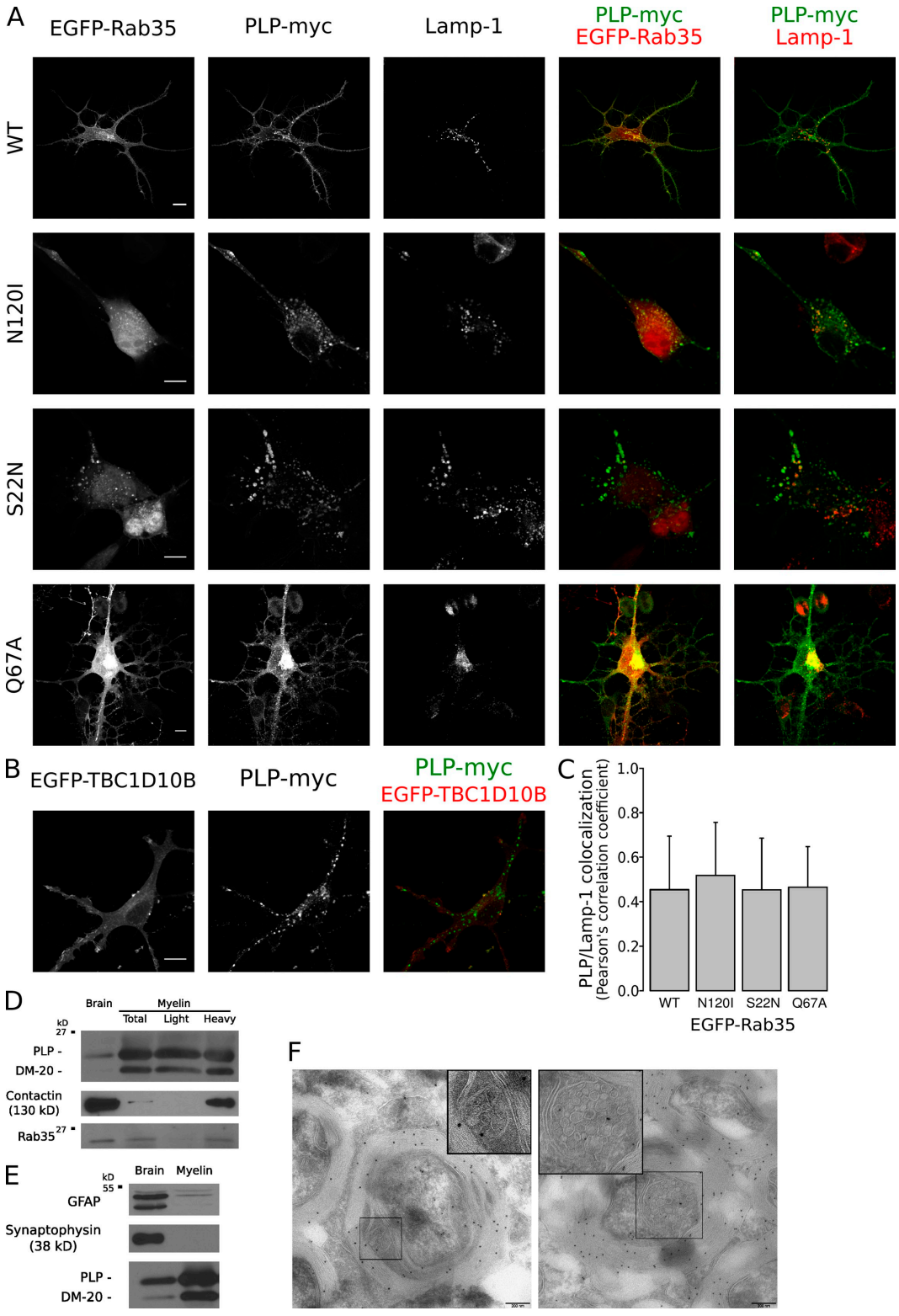


Figure 4. **Localization of Rab35.** (A) Oli-neu cells were transfected with PLP-myc together with EGFP-Rab35$^{S22N}$, EGFP-Rab35$^{N120I}$, EGFP-Rab35$^{Q67A}$, or wild-type EGFP-Rab35 (WT) and analyzed by confocal microscopy. Wild-type and the GTP-locked Rab35$^{Q67A}$ were detected at the plasma membrane, whereas the GDP-locked Rab35$^{S22N}$ and the nucleotide-empty EGFP-Rab35$^{N120I}$ were mainly found within the cytosol and in vesicles that contained PLP and Lamp-1. (B) Oli-neu cells were cotransfected with EGFP-TBC1D10B and PLP-myc and analyzed by confocal microscopy. (C) Quantification of colocalization of PLP with Lamp-1 within 7 × 7–μm intracellular regions after coexpression with the different protein Rab35 mutants is shown ($n$ = ~27–38). The values represent the mean ± SD. (D) Myelin (total) and myelin subfractions (light and heavy) were purified from the brain homogenates (brain) of adult mice, and the amounts of Rab35, PLP/DM20, and contactin were determined by Western blotting. Rab35 was detected in purified myelin (total) and in the subfraction of higher density (heavy). (E) Purified myelin did not contain relevant levels of GFAP or synaptophysin proteins, confirming the purity of isolated myelin. (F) Immunoelectron microscopy analysis of myelin in the spinal cord of adult mice with PLP antibodies. The left image shows an MVB within a cytoplasmic channel of compact myelin, and the right image shows an MVB in the abaxonal space. MVBs (boxed areas) are displayed at higher magnification in the insets. Bars: (A and B) 10 μm; (F) 200 nm.

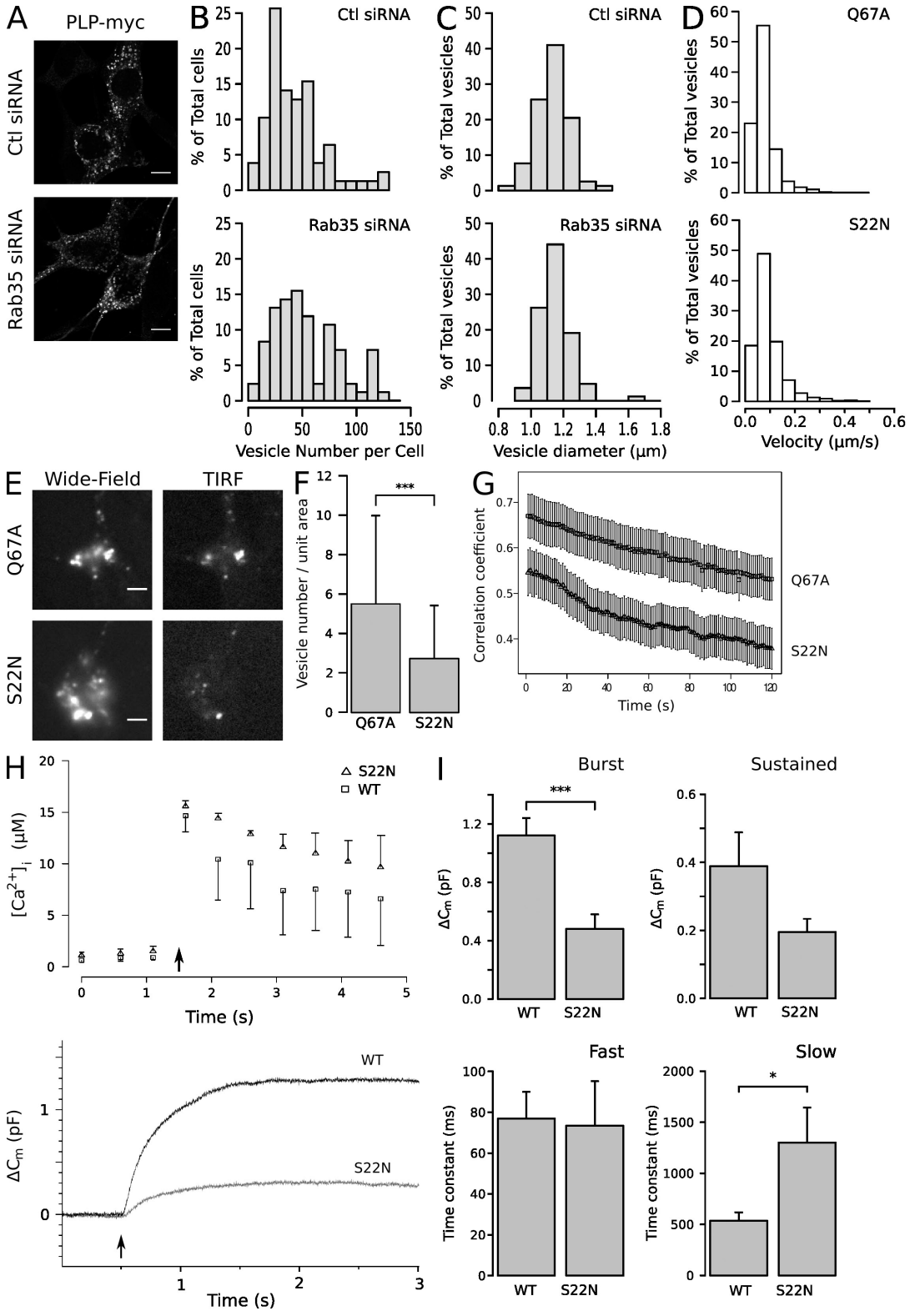


Figure 5. **Rab35 functions in recruitment of the endosomal vesicle to the plasma membrane.** (A) Control (Ctl) or siRNA against Rab35 was delivered into cells by nucleofection, and the cells were imaged by immunofluorescence microscopy to detect PLP-myc. (B and C) Vesicle number and size are displayed in a histogram. Note that vesicle size was unaffected, whereas the number of vesicles increased after Rab35 knockdown ($n = \sim$80 cells from three independent experiments). (D) To analyze vesicular movement, PLP-myc was cotransfected with wild-type or mutant EGFP-tagged Rab35, cells were stained with LysoTracker red DND-99, and time-lapse images were acquired at 1 frame every 2 s at 37°C. The motility of LysoTracker-labeled vesicles was slightly reduced when active GTP-locked Rab35$^{Q67A}$ was expressed ($n = \sim$1,800 vesicles from three independent experiments). (E and F) The mean number of LysoTracker green DND-26–labeled vesicles in a field of 12.7 µm × 12.7 µm (unit area) was determined in the evanescent excitation field. Expression of the GTP-locked Rab35$^{Q67A}$ increased the number of vesicles in the TIRF evanescence field as compared with the GDP-locked Rab35$^{S22N}$ ($n = 70$ cells from three independent experiments; mean ± SD; ***, $P < 0.001$; Welch's two-sample $t$ test). (G) The mobility of LysoTracker green DND-26–labeled vesicles

two-sample *t* test; Fig. 5 D). One possible explanation is that Rab35$^{Q67A}$ promotes vesicle docking/tethering. To test this possibility, cells were imaged with total internal reflection fluorescence (TIRF) microscopy to observe the vesicles just beneath the plasma membrane. Indeed, we found that that Rab35$^{Q67A}$ increased the number of LysoTracker-labeled vesicles within the evanescent excitation field (~120 nm) by around 50% as compared with GDP-locked Rab35$^{S22N}$ (Fig. 5, E and F). To determine whether these vesicles were docked/tethered to the plasma membrane, we performed time-lapse TIRF experiments. To estimate vesicle motility, the temporal colocalization was determined by calculating the Pearson's correlation coefficient of pairs of images separated by time (Huang et al., 2007). In such an analysis, the degree of temporal colocalization is inversely related to vesicle motility. Expression of Rab35$^{Q67A}$ increased vesicle immobilization as compared with the inactive form of Rab35 (Fig. 5 G).

Because exosome release is known to be stimulated by intracellular $Ca^{2+}$ levels (Savina et al., 2003; Krämer-Albers et al., 2007), we determined vesicular fusion after $Ca^{2+}$ stimulation by whole-cell capacitance measurements ($C_m$; Voets, 2000). Cells were held in whole-cell patch-clamp configuration and dialyzed through the pipette with the $Ca^{2+}$-caged nitrophenyl (NP)-EGTA and a mixture of two $Ca^{2+}$-sensitive fluorescent dyes, Fura-4 and -2FF, which allows us to precisely measure $[Ca^{2+}]_i$ over a large concentration range (Voets, 2000). 2–3 min after the whole-cell configuration, a strong UV flash was applied to the cells, causing the photolysis of NP-EGTA and leading to a step-like homogenous increase of $[Ca^{2+}]_i$. After flash photolysis, the change in $C_m$ consisted of a fast initial phase, the exocytic burst, followed by a slower sustained phase of secretion, which is similar but slower to what has been reported in other cell types (Fig. 5 H; Voets, 2000). The exocytic burst component represents the readily releasable pool (RRP), whereas the sustained component represents the recruitment of fusion component vesicles from a reserve pool. In cells overexpressing a dominant-negative mutant of Rab35 (Rab35$^{S22N}$), the mean RRP size in mutant cells was markedly smaller than that of wild-type Rab35-expressing cells (Rab35: 1.12 ± 0.12 pF, $n = 15$; Rab35$^{S22N}$: 0.48 ± 0.10 pF, $n = 11$; $P < 0.001$; Fig. 5 I). Interestingly, although the release kinetics of RRP (during 0–1 s) was identical, the size of RRP of was reduced in Rab35$^{S22N}$ as compared with wild-type Rab35-expressing cells (Rab35: 76.9 ± 13.1 ms, $n = 10$; Rab35$^{S22N}$: 73.4 ± 21.8 ms, $n = 5$; $P > 0.05$; Fig. 5 I). In addition, the time constant of the slow component increased significantly after expression of Rab35$^{S22N}$ (Rab35: 535.9 ± 81.2 ms, $n = 10$; Rab35$^{S22N}$: 1,300.4 ± 344.1 ms, $n = 5$; $P < 0.05$). Although these data do not distinguish the vesicle population undergoing fusion, they do show a role of Rab35 in a $Ca^{2+}$-regulated pathway of vesicle fusion with the plasma membrane.

In summary, we provide new evidence that Rab35 and its GAPs TBC1D10A–C regulate exosome release of PLP in oligodendroglial cells, possibly by controlling the docking/tethering of endocytic vesicles with the plasma membrane. The functional involvement of Rab35 in an endocytic recycling pathway is consistent with previous studies demonstrating a role for Rab35 in the recycling of transferrin and yolk receptors in HeLa cells and *Caenorhabditis elegans*, respectively (Kouranti et al., 2006; Sato et al., 2008). Although a previous study indicates that Rab35 controls a fast recycling pathway from peripheral endocytic compartments to the plasma membrane (Sato et al., 2008), our work implies that Rab35 also acts on late endosomes/MVBs. Rab11, a well-known regulator of endosomal recycling, has also been linked to the control of exosome release in K562a cells (Savina et al., 2005). Interestingly, work in *C. elegans* showed that the combined knockdown of Rab35 and -11 leads to a dramatic enhancement of intracellular accumulation of endosomal cargo (Sato et al., 2008). Thus, it is plausible that Rab35 and -11 play a dual role in endocytic recycling rather than acting in sequential stages. Further work will be required to define the precise functional contributions of Rab35 and -11 in exosome biogenesis. It will also be important to find out whether the machinery involved in exosome secretion is related to the one required for the biogenesis of secretory lysosomes or melanosomes (Stinchcombe and Griffiths, 2007; Idone et al., 2008; Delevoye et al., 2009). Interestingly, a recent study shows that Rab27 not only functions in melanosome biogenesis but also in the exosome secretion pathway (Ostrowski et al., 2010). Together with this study, these findings provide a molecular basis for understanding MVB trafficking and exosome biogenesis. This is important as these vesicles have been implicated in various different cellular functions (e.g., intercellular signaling and transfer of mRNA) and disease states (e.g., prion disease and tumor spreading). Thus, strategies to interfere with their biogenesis such as blocking Rab35 function will be important to get a better understanding of their physiological and pathological relevance. The function of glial-derived exosomes is also unclear. The finding that MVBs are not only found in the soma and the processes of oligodendrocytes but also within the periaxonal space of myelin points to the interesting possibility that they transfer cargo into the axon. The identification and characterization of Rab35 effectors is likely to yield new insights into how exosomes are generated and where the release occurs.

## Materials and methods

### Antibodies, plasmids, and other reagents

The following primary antibodies were used: rat anti–Lamp-1 (CD107a; BD), rabbit anti-myc (Millipore), mouse anti-HA (16B12; Covance), mouse anti-PLP (3F4; a gift from K.-A. Nave, Max Planck Institute for Experimental

was determined by time-lapse TIRF microscopy and analyzed by calculating the temporal correlation coefficient between pairs of images separated by time. The degree of temporal colocalization is inversely related to vesicle motility ($n = \sim 35$ videos from three independent experiments; mean ± SEM). (H) Representative traces of intracellular $Ca^{2+}$ concentration (top) and membrane capacitance (bottom) in response to flash photolysis of caged $Ca^{2+}$ (indicated by arrows) in cells expressing wild-type (black trace) and GDP-locked Rab35$^{S22N}$ (gray trace). Error bars represent SEM. (I) A decrease in capacitance during the exocytotic burst (0–1 s) and an increase in time constant of the slow compartment were observed in cells expressing Rab35$^{S22N}$ (*, $P < 0.05$; ***, $P < 0.001$; Mann-Whitney test; mean ± SEM). Bars: (A) 10 µm; (E) 5 µm.

Medicine, Göttingen, Germany), mouse anticontactin (K67/25; NeuroMab), rabbit anti-Rab35 (a gift from A. Echard, Institut Curie, Paris, France), rabbit anti-GFAP (Promega), mouse antisynaptophysin (Synaptic Systems), rabbit anti-GFP (Abcam; Invitrogen), mouse anti-myc (Cell Signaling Technology), and mouse antiactin (AC-40; Sigma-Aldrich). Secondary antibodies were purchased from Dianova. The following expression plasmids were used: EGFP–Rab GAPs and their catalytically inactive mutants (Haas et al., 2005), EGFP–Rab GTPases and their mutants (Yoshimura et al., 2007), GFP-Rab7 and -Rab7$^{T22N}$ (provided by M. Zerial, Max Planck Institute of Molecular Cell Biology and Genetics, Dresden, Germany), pEYFP-C1 (BD), and PLP-myc and -EGFP (Trajkovic et al., 2008). Colloidal gold conjugates to protein A were obtained from the Cell Microscopy Center, University Medical Center Utrecht, Utrecht, Netherlands.

To produce DsRed2-Rab35 and its constitutively active and inactive mutations, Rab35 sequences were amplified from pEGFP-Rab35 plasmids with PCR (primers, 5′-TTAAGCTTCGATGGCCCGGGACTACGACC-3′ and 5′-TTGGATCCTTAGCAGCAGCGTTTCTTTCGTTTACTG-3′), restriction digested, and inserted into the pDsRed2-C1 plasmid (Invitrogen) between the HindIII and BamHI restriction sites.

### MS

Exosomes purified from Oli-neu cell lines were separated by a 4–12% Bis-Tris gradient NuPAGE gel (Invitrogen) and stained with Colloidal blue (Invitrogen). Each gel lane was cut into 25 slices, and proteins were in-gel digested with trypsin. Tryptic peptides were analyzed on an LTQ XL Orbitrap (Thermo Fisher Scientific) coupled to an LC system (1100 series; Agilent Technologies). Peptides were separated at a flow rate of 200 nl/min on a reversed phase column ($C_{18}$; Reprosil). Elution of the peptides was performed with a 50-min gradient from 7–40% mobile phase B (80% acetonitrile and 0.15% formic acid). Peak lists were searched against the National Center for Biotechnology Information nonredundant database using Mascot version 2.2 (Matrix Science, Inc.) as a search engine. Mass accuracy was 5 ppm for both parent ion and fragment ions. The peptides were constrained to be tryptic with a maximum of two missed cleavages. Carbamidomethylation of cysteines was considered a fixed modification, whereas oxidation of methionine residues was considered a variable modification. The proteins found in our exosome preparation were compared with proteins identified previously in exosomes from other cell types (Barile et al., 2005; Segura et al., 2005; Aoki et al., 2007; Valadi et al., 2007; Conde-Vancells et al., 2008).

### Cell culture, transfection, and RNAi

The oligodendroglial precursor cell line Oli-neu (provided by J. Trotter, University of Mainz, Mainz, Germany) was cultured as previously described (Trajkovic et al., 2006). The cells were seeded on poly-L-lysine–precoated plastic Petri dishes or glass coverslips and cultured at 37°C with 5% $CO_2$ in SATO medium supplied with 5% horse serum. Transient transfections were performed using TransIT-LT1 transfection reagent (Mirus) according to the manufacturer's instructions. siRNA was delivered into Oli-neu cells by electrophoresis with a Basic Neuron Nucleofector kit (Lonza) in a two-step fashion as previously described (Trajkovic et al., 2006). For RNAi, we used the pooled oligonucleotides targeting four sequences of mouse Rab35 (L-042604-01) and the pooled nontargeting oligonucleotides (D-001810-10) as control from Thermo Fisher Scientific.

### Exosome purification

Exosomes were prepared as described previously (Trajkovic et al., 2008). Before the preparation, the culture medium was replaced by serum-free medium, and media were then collected and centrifuged for 10 min at 3,000 *g* and two times for 10 min at 4,000 *g* before subjecting it for ultracentrifugation at 10,000 *g* for 30 min and at 100,000 *g* for 1 h. The pellets were resuspended in sample buffer (20% glycerol, 4 mM EDTA, 4% SDS, 4% 2-mercaptoethanol, and 100 mM Tris-HCl, pH 6.8). Cell lysates were incubated for 10 min on ice with lysis buffer (2% Nonidet P-40, 0.2% SDS, and 1 mM EGTA in PBS supplied with Complete protease inhibitor cocktail from Roche), scraped, and centrifuged at 10,000 *g* for 10 min. A fraction of the supernatant was mixed with sample buffer before subjecting it to 10 or 12% SDS-PAGE and transfer to nitrocellulose membranes. Western blots were revealed by enhanced chemiluminescence (Thermo Fisher Scientific), and bands were quantified using ImageJ software (National Institutes of Health).

### Rab GAP assays

Rab GAP assays using recombinant hexahistidine-GST–tagged human Rab GTPases and hexahistidine-tagged TBC1D10 family proteins were performed as described previously (Haas et al., 2005; Fuchs et al., 2007; Yoshimura et al., 2007). All proteins tested corresponded to the full-length open reading frames. In brief, standard assays were performed for 60 min at 37°C, using 100 pmol γ-[$^{32}$P]GTP preloaded GST-Rab and 10 pmol hexahistidine-tagged TBC1D10A, -B, or -C. Released inorganic phosphate was taken as a measure of GTP hydrolysis in picomoles per hour.

In our initial experiments of Rab GAPs, we observed some activity of more than one GAP toward Rab35; however, unlike TBC1D10A–C none of these was specific for Rab35. This was because of a C-terminal cleavage that occurs during preparation of the recombinant Rab35 protein. An altered preparation method using low temperature expression for shorter time yields predominantly full-length Rab35. This altered method was used in Yoshimura et al. (2007) and resolved the problems we had observed relating to nonspecific activation of Rab35.

### Immunofluorescence, microscopy, and image analysis

Immunofluorescence was performed as described previously (Trajkovic et al., 2006). Before the primary and fluorescent secondary antibody labeling, the cells were fixed with 4% paraformaldehyde in PBS, washed, and permeabilized with 0.1% Triton X-100 for 1 min. Fluorescence images were acquired with a wide-field fluorescence microscope (DMRXA; Leica) through a 40× HCX Plan-Fluotar objective (Leica) or a confocal microscope setup and its software (LSM 510 [Carl Zeiss, Inc.]; or TCS SP2 AOBS [Leica]) with a 63× NA 1.4 oil Plan-Apochromat objective (Carl Zeiss, Inc.).

TIRF microscopy was performed with a prism-based setup. The images were acquired with a camera (Cascade 512B; Photometrics) on a microscope (Axiovert 135; Carl Zeiss, Inc.) with a 63× water-immersed objective (Leica; pixel size, ∼0.25 × 0.25 µm). The excitation light was generated with an argon laser (488 nm), and the fluorescence emission signals were filtered with an HQ 515/30 band-pass filter. Wide-field fluorescence images were obtained with the same capturing settings as the TIRF images, using a 450–490 band-passed excitation light generated with a monochromator.

To analyze vesicular movement, PLP-myc was cotransfected with wild-type or mutant EGFP-tagged Rab35, and cells were stained with 50 nM LysoTracker red DND-99 (Invitrogen) for 10 min 24–30 h after transfection and washed with imaging medium (160 mM NaCl, 4.5 mM Kcl, 2 mM $CaCl_2$, 1 mM $MgCl_2$, 10 mM glucose, and 10 mM Hepes, pH 7.4), and the time-lapse images were acquired with a TCS SP2 AOBS confocal microscope at 1 frame every 2 s at 37°C. The pinhole was set at 300 µm, and a pixel size of 0.12 µm × 0.12 µm was used.

The velocities of the vesicles were automatically analyzed using a previously described algorithm with MATLAB (The MathWorks, Inc.; Westphal et al., 2008). The images were smoothened by convolution with a Gaussian function of 2 pixels full width at half maximum, and vesicles were found as the local maxima, which exceed a threshold of 20% relative to the brightest object. Vesicles were tracked by minimizing the sum of the squared distances moved of all particles. The maximally allowed speed of a particle was 8 pixels/frame.

For PLP/Lamp-1 colocalization assay, an 8-bit confocal image with a resolution of 0.071 µm/pixel of a 7-µm × 7-µm intracellular region was obtained; signals of PLP-myc and Lamp-1 channels of the image were subjected to a calculation using a self-written ImageJ plugin for Pearson's correlation coefficient. To calculate vesicle size and number, confocal images with the aforementioned pixel size of a 73-µm × 73-µm field were taken and analyzed with ImageJ. For the correlation change in image series acquired with the TIRF microscope, an image region of 15.2 µm × 15.2 µm containing cells expressing DsRed2-Rab35, identified in the wide-field fluorescence channel, was cropped, and Pearson's correlation coefficient was calculated between pairs of images separated by time (first frame and the following frames within the video sequence).

### Capacitance and $Ca^{2+}$ measurements

Experimental procedures for whole-cell patch-clamp and capacitance measurements were performed essentially as described previously (Voets, 2000). Mounted cells were patched with 3–4 MΩ pipettes while perfused with extracellular solution. The Lindau-Neher technique was used for the capacitance measurements, and the data were acquired with the high time resolution PULSE software (HEKA). In the flash experiments, cells were cotransfected with PLP-myc and wild-type or mutant EGFP-tagged Rab35 for 16–20 h. Exocytosis was elicited by photorelease of caged $Ca^{2+}$ (NP-EGTA), which was preloaded into the cell via the patch pipette. Flashes of UV light were generated by a flash lamp (Dr. Rapp Optoelektronik) and coupled to an inverted microscope (Axiovert 200; Carl Zeiss, Inc.). Fluorescence excitation light was generated by a monochromator (Polychrome II;

TILL Photonics), and a two-port epifluorescence condenser was used for coupling 80% of the flash light and 20% of the monochromator light into the microscope. Cells were bathed in extracellular solution (140 mM NaCl, 2.8 mM KCl, 4 mM $CaCl_2$, 41 mM $MgCl_2$, 10 mM Na-Hepes, and 2 mg/ml glucose, pH 7.2; osmolarity ~310 mosM) and patched using a pipette solution containing the photolysable $Ca^{2+}$ chelator NP-EGTA (110 mM Cs-glutamate, 20 mM Cs-Hepes, 2 mM Mg-ATP, 8 mM NaCl, 0.3 mM Na-GTP, 10 mM NP-EGTA, 9 mM $CaCl_2$, 400 µM Fura-4F [Invitrogen], 400 µM Furaptra [Invitrogen], pH 7.2; osmolarity, ~300 mosM). $Ca^{2+}$ measurements were performed by dual-wavelength ratiometric fluorometry as described previously (Voets, 2000) using a 1:1 mixture of the $Ca^{2+}$-sensitive dyes Fura-4F ($K_d$ = 1 µM) and Furaptra ($K_d$ = 40 µM). The signal (ratio of fluorescence with excitation at 350 and 380 nm) was calibrated intracellularly by dialyzing the cells in whole-cell configuration with eight different pipette solutions with known $[Ca^{2+}]_i$. $Ca^{2+}$ ramps were elicited by the fluorescence excitation light, alternating between 350 and 380 nm, so that photolysis of NP-EGTA could be combined with simultaneous measurement of $[Ca^{2+}]_i$. All measurements were performed at room temperature. Data analysis was performed using Axograph software (Axograph Scientific), and results were presented as mean ± SEM with the indicated number of experiments. Statistical significance was evaluated using the Mann-Whitney test. $P < 0.05$ was considered to be statistically significant.

### Myelin preparation

The myelin preparation was performed essentially as described previously (Larocca and Norton, 2007). In brief, the brains from 3–6-mo-old mice were homogenized in PBS containing protease inhibitors by sonication. The brain homogenate was put on top of two-step sucrose gradients (0.32 and 0.85 M sucrose in preparation buffer containing 5 mM EDTA and 10 mM Hepes, pH 7.4). After the gradients were centrifuged at 75,000 *g* for 30 min, the interfaces were collected, diluted at least 10 times with $H_2O$, and centrifuged at 75,000 *g* for 20 min. The pellet was washed twice with $H_2O$ and recovered by 10-min centrifugations at 12,000 *g* (crude myelin), and the protocol was repeated to obtain purified myelin.

To separate the heavy and light myelin (Rios et al., 2000), the crude myelin pellet was resuspended with preparation buffer, put on top of a three-step sucrose gradient (0.32, 0.62, and 0.8 M sucrose in preparation buffer), and centrifuged at 75,000 *g* for 30 min. The light and heavy myelin fractions were collected at the 0.32/0.62 M and 0.62/0.8 M sucrose interfaces, respectively. The fractions were washed with $H_2O$ and recovered by centrifugations for 20 min at 75,000 *g* and twice for 10 min at 12,000 *g*. The protein concentrations of the brain homogenate and myelin preparations were determined by the Bradford assay.

### EGF degradation

The EGF degradation assay was performed as described previously (Trajkovic et al., 2008). Cells transfected with EGFP-tagged EGF receptor (EGFR-EGFP) were incubated with 50 ng/ml Alexa Fluor 555–labeled EGF (Invitrogen) for 15 min, washed, and incubated for 4 h in conditioned culture medium to allow EGF degradation. For quantification, images of randomly selected transfected cells were recorded at fixed settings below pixel-value saturation, and fluorescence intensities were quantified using Meta Imaging Series 6.1 software (MDS Analytical Technologies).

### Immunoelectron microscopy

Immunoelectron microscopy was performed as described previously (Werner et al., 2007). Mice were fixed by transcardial perfusion with 4% formaldehyde and 0.2% glutaraldehyde in 0.1 M phosphate buffer containing 0.5% NaCl. Dissected optic nerves were infiltrated in 2.3 M sucrose in 0.1 M phosphate buffer overnight, mounted onto aluminum pins for ultramicrotomy, and frozen in liquid nitrogen. Ultrathin cryosections were picked up according to Liou et al. (1996) in a 1:1 mixture of 2% methylcellulose and 2.3 M sucrose. For immunolabeling, sections were incubated with antibodies specific for PLP, which was detected with protein A–gold (10 nm). Sections were analyzed with a LEO EM912 Omega (Carl Zeiss, Inc.), and digital micrographs were obtained with an on-axis 2,048 × 2,048–pixel charge-coupled device camera (Proscan).

### Statistical analysis

The significance of data was evaluated with the statistical program R using Welch's two-sample *t* test or one-sample *t* test.

### Online supplemental material

Fig. S1 shows the analysis of Rab GTPases (identified in the MS analysis) in the exosomal membrane fraction. Fig. S2 shows the subcellular localization of Rab35 in HeLa cells. Fig. S3 shows the inhibition of EGF degradation by dominant-negative Rab7 but not Rab35. Table S1, included as an Excel file, shows the MS analysis of Oli-neu–derived exosomes. Online supplemental material is available at http://www.jcb.org/cgi/content/full/jcb.200911018/DC1.

We are grateful to A. Echard for the Rab35 antibody (a gift to M. Grønborg, R. Jahn laboratory). We thank K.-A. Nave for his generous support and H. Urlaub for the mass spectrometric analysis of the samples. We also thank T. Kohl for help with the TIRF experiments and N. Pavlos for comments on the manuscript.

This work was supported by grants from the Deutsche Forschungsgemeinschaft (SFB 523, GRK 521) and the European Molecular Biology Organization Young Investigators Programme and a European Research Council Starting Grant to M. Simons and a Wellcome Trust programme grant to F.A. Barr.

Submitted: 2 November 2009
Accepted: 19 March 2010

## References

Aoki, N., S. Jin-no, Y. Nakagawa, N. Asai, E. Arakawa, N. Tamura, T. Tamura, and T. Matsuda. 2007. Identification and characterization of microvesicles secreted by 3T3-L1 adipocytes: redox- and hormone-dependent induction of milk fat globule-epidermal growth factor 8-associated microvesicles. *Endocrinology*. 148:3850–3862. doi:10.1210/en.2006-1479

Barile, M., T. Pisitkun, M.J. Yu, C.L. Chou, M.J. Verbalis, R.F. Shen, and M.A. Knepper. 2005. Large scale protein identification in intracellular aquaporin-2 vesicles from renal inner medullary collecting duct. *Mol. Cell. Proteomics*. 4:1095–1106. doi:10.1074/mcp.M500049-MCP200

Barres, B.A. 2008. The mystery and magic of glia: a perspective on their roles in health and disease. *Neuron*. 60:430–440. doi:10.1016/j.neuron.2008.10.013

Buschow, S.I., E.N. Nolte-'t Hoen, G. van Niel, M.S. Pols, T. ten Broeke, M. Lauwen, F. Ossendorp, C.J. Melief, G. Raposo, R. Wubbolts, et al. 2009. MHC II in dendritic cells is targeted to lysosomes or T cell-induced exosomes via distinct multivesicular body pathways. *Traffic*. 10:1528–1542. doi:10.1111/j.1600-0854.2009.00963.x

Conde-Vancells, J., E. Rodriguez-Suarez, N. Embade, D. Gil, R. Matthiesen, M. Valle, F. Elortza, S.C. Lu, J.M. Mato, and J.M. Falcon-Perez. 2008. Characterization and comprehensive proteome profiling of exosomes secreted by hepatocytes. *J. Proteome Res.* 7:5157–5166. doi:10.1021/pr8004887

Delevoye, C., I. Hurbain, D. Tenza, J.B. Sibarita, S. Uzan-Gafsou, H. Ohno, W.J. Geerts, A.J. Verkleij, J. Salamero, M.S. Marks, and G. Raposo. 2009. AP-1 and KIF13A coordinate endosomal sorting and positioning during melanosome biogenesis. *J. Cell Biol.* 187:247–264. doi:10.1083/jcb.200907122

Fuchs, E., A.K. Haas, R.A. Spooner, S. Yoshimura, J.M. Lord, and F.A. Barr. 2007. Specific Rab GTPase-activating proteins define the Shiga toxin and epidermal growth factor uptake pathways. *J. Cell Biol.* 177:1133–1143. doi:10.1083/jcb.200612068

Gruenberg, J., and H. Stenmark. 2004. The biogenesis of multivesicular endosomes. *Nat. Rev. Mol. Cell Biol.* 5:317–323. doi:10.1038/nrm1360

Haas, A.K., E. Fuchs, R. Kopajtich, and F.A. Barr. 2005. A GTPase-activating protein controls Rab5 function in endocytic trafficking. *Nat. Cell Biol.* 7:887–893. doi:10.1038/ncb1290

Huang, S., L.M. Lifshitz, C. Jones, K.D. Bellve, C. Standley, S. Fonseca, S. Corvera, K.E. Fogarty, and M.P. Czech. 2007. Insulin stimulates membrane fusion and GLUT4 accumulation in clathrin coats on adipocyte plasma membranes. *Mol. Cell. Biol.* 27:3456–3469. doi:10.1128/MCB.01719-06

Idone, V., C. Tam, and N.W. Andrews. 2008. Two-way traffic on the road to plasma membrane repair. *Trends Cell Biol.* 18:552–559. doi:10.1016/j.tcb.2008.09.001

Itoh, T., and M. Fukuda. 2006. Identification of EPI64 as a GTPase-activating protein specific for Rab27A. *J. Biol. Chem.* 281:31823–31831. doi:10.1074/jbc.M603808200

Korkut, C., B. Ataman, P. Ramachandran, J. Ashley, R. Barria, N. Gherbesi, and V. Budnik. 2009. Trans-synaptic transmission of vesicular Wnt signals through Evi/Wntless. *Cell*. 139:393–404. doi:10.1016/j.cell.2009.07.051

Kouranti, I., M. Sachse, N. Arouche, B. Goud, and A. Echard. 2006. Rab35 regulates an endocytic recycling pathway essential for the terminal steps of cytokinesis. *Curr. Biol.* 16:1719–1725. doi:10.1016/j.cub.2006.07.020

Krämer-Albers, E.M., N. Bretz, S. Tenzer, C. Winterstein, W. Möbius, H. Berger, K.-A. Nave, H. Schild, and J. Trotter. 2007. Oligodendrocytes secrete

exosomes containing major myelin and stress-protective proteins: Trophic support for axons? *Proteomics-Clinical Applications*. 1:1446–1461. doi:10.1002/prca.200700522

Lakkaraju, A., and E. Rodriguez-Boulan. 2008. Itinerant exosomes: emerging roles in cell and tissue polarity. *Trends Cell Biol.* 18:199–209. doi:10.1016/j.tcb.2008.03.002

Lanzetti, L., V. Rybin, M.G. Malabarba, S. Christoforidis, G. Scita, M. Zerial, and P.P. Di Fiore. 2000. The Eps8 protein coordinates EGF receptor signalling through Rac and trafficking through Rab5. *Nature*. 408:374–377. doi:10.1038/35042605

Larocca, J.N., and W.T. Norton. 2007. Isolation of myelin. *Curr. Protoc. Cell Biol.* Chapter 3:Unit 3.25. doi:10.1002/0471143030.cb0325s33

Liou, W., H.J. Geuze, and J.W. Slot. 1996. Improving structural integrity of cryosections for immunogold labeling. *Histochem. Cell Biol.* 106: 41–58. doi:10.1007/BF02473201

Ostrowski, M., N.B. Carmo, S. Krumeich, I. Fanget, G. Raposo, A. Savina, C.F. Moita, K. Schauer, A.N. Hume, R.P. Freitas, et al. 2010. Rab27a and Rab27b control different steps of the exosome secretion pathway. *Nat. Cell Biol.* 12:19–30: 1–13. doi:10.1038/ncb2000

Patino-Lopez, G., X. Dong, K. Ben-Aissa, K.M. Bernot, T. Itoh, M. Fukuda, M.J. Kruhlak, L.E. Samelson, and S. Shaw. 2008. Rab35 and its GAP EPI64C in T cells regulate receptor recycling and immunological synapse formation. *J. Biol. Chem.* 283:18323–18330. doi:10.1074/jbc.M800056200

Piper, R.C., and D.J. Katzmann. 2007. Biogenesis and function of multivesicular bodies. *Annu. Rev. Cell Dev. Biol.* 23:519–547. doi:10.1146/annurev.cellbio.23.090506.123319

Rios, J.C., C.V. Melendez-Vasquez, S. Einheber, M. Lustig, M. Grumet, J. Hemperly, E. Peles, and J.L. Salzer. 2000. Contactin-associated protein (Caspr) and contactin form a complex that is targeted to the paranodal junctions during myelination. *J. Neurosci.* 20:8354–8364.

Salzer, J.L. 2003. Polarized domains of myelinated axons. *Neuron*. 40:297–318. doi:10.1016/S0896-6273(03)00628-7

Sato, M., K. Sato, W. Liou, S. Pant, A. Harada, and B.D. Grant. 2008. Regulation of endocytic recycling by *C. elegans* Rab35 and its regulator RME-4, a coated-pit protein. *EMBO J.* 27:1183–1196. doi:10.1038/emboj.2008.54

Savina, A., M. Furlán, M. Vidal, and M.I. Colombo. 2003. Exosome release is regulated by a calcium-dependent mechanism in K562 cells. *J. Biol. Chem.* 278:20083–20090. doi:10.1074/jbc.M301642200

Savina, A., C.M. Fader, M.T. Damiani, and M.I. Colombo. 2005. Rab11 promotes docking and fusion of multivesicular bodies in a calcium-dependent manner. *Traffic*. 6:131–143. doi:10.1111/j.1600-0854.2004.00257.x

Schorey, J.S., and S. Bhatnagar. 2008. Exosome function: from tumor immunology to pathogen biology. *Traffic*. 9:871–881. doi:10.1111/j.1600-0854.2008.00734.x

Segura, E., C. Nicco, B. Lombard, P. Véron, G. Raposo, F. Batteux, S. Amigorena, and C. Théry. 2005. ICAM-1 on exosomes from mature dendritic cells is critical for efficient naive T-cell priming. *Blood*. 106:216–223. doi:10.1182/blood-2005-01-0220

Sherman, D.L., and P.J. Brophy. 2005. Mechanisms of axon ensheathment and myelin growth. *Nat. Rev. Neurosci.* 6:683–690. doi:10.1038/nrn1743

Simons, M., and G. Raposo. 2009. Exosomes—vesicular carriers for intercellular communication. *Curr. Opin. Cell Biol.* 21:575–581. doi:10.1016/j.ceb.2009.03.007

Simons, M., and J. Trotter. 2007. Wrapping it up: the cell biology of myelination. *Curr. Opin. Neurobiol.* 17:533–540. doi:10.1016/j.conb.2007.08.003

Stenmark, H. 2009. Rab GTPases as coordinators of vesicle traffic. *Nat. Rev. Mol. Cell Biol.* 10:513–525. doi:10.1038/nrm2728

Stinchcombe, J.C., and G.M. Griffiths. 2007. Secretory mechanisms in cell-mediated cytotoxicity. *Annu. Rev. Cell Dev. Biol.* 23:495–517. doi:10.1146/annurev.cellbio.23.090506.123521

Théry, C., M. Ostrowski, and E. Segura. 2009. Membrane vesicles as conveyors of immune responses. *Nat. Rev. Immunol.* 9:581–593. doi:10.1038/nri2567

Trajkovic, K., A.S. Dhaunchak, J.T. Goncalves, D. Wenzel, A. Schneider, G. Bunt, K.A. Nave, and M. Simons. 2006. Neuron to glia signaling triggers myelin membrane exocytosis from endosomal storage sites. *J. Cell Biol.* 172:937–948. doi:10.1083/jcb.200509022

Trajkovic, K., C. Hsu, S. Chiantia, L. Rajendran, D. Wenzel, F. Wieland, P. Schwille, B. Brügger, and M. Simons. 2008. Ceramide triggers budding of exosome vesicles into multivesicular endosomes. *Science*. 319: 1244–1247. doi:10.1126/science.1153124

Trapp, B.D., S.B. Andrews, C. Cootauco, and R. Quarles. 1989. The myelin-associated glycoprotein is enriched in multivesicular bodies and periaxonal membranes of actively myelinating oligodendrocytes. *J. Cell Biol.* 109:2417–2426. doi:10.1083/jcb.109.5.2417

Valadi, H., K. Ekström, A. Bossios, M. Sjöstrand, J.J. Lee, and J.O. Lötvall. 2007. Exosome-mediated transfer of mRNAs and microRNAs is a novel mechanism of genetic exchange between cells. *Nat. Cell Biol.* 9:654–659. doi:10.1038/ncb1596

Voets, T. 2000. Dissection of three Ca2+-dependent steps leading to secretion in chromaffin cells from mouse adrenal slices. *Neuron*. 28:537–545. doi:10.1016/S0896-6273(00)00131-8

Walseng, E., O. Bakke, and P.A. Roche. 2008. Major histocompatibility complex class II-peptide complexes internalize using a clathrin- and dynamin-independent endocytosis pathway. *J. Biol. Chem.* 283:14717–14727. doi:10.1074/jbc.M801070200

Werner, H.B., K. Kuhlmann, S. Shen, M. Uecker, A. Schardt, K. Dimova, F. Orfaniotou, A. Dhaunchak, B.G. Brinkmann, W. Möbius, et al. 2007. Proteolipid protein is required for transport of sirtuin 2 into CNS myelin. *J. Neurosci.* 27:7717–7730. doi:10.1523/JNEUROSCI.1254-07.2007

Westphal, V., S.O. Rizzoli, M.A. Lauterbach, D. Kamin, R. Jahn, and S.W. Hell. 2008. Video-rate far-field optical nanoscopy dissects synaptic vesicle movement. *Science*. 320:246–249. doi:10.1126/science.1154228

Yoshimura, S., J. Egerer, E. Fuchs, A.K. Haas, and F.A. Barr. 2007. Functional dissection of Rab GTPases involved in primary cilium formation. *J. Cell Biol.* 178:363–369. doi:10.1083/jcb.200703047

Zhang, J., M. Fonovic, K. Suyama, M. Bogyo, and M.P. Scott. 2009. Rab35 controls actin bundling by recruiting fascin as an effector protein. *Science*. 325:1250–1254. doi:10.1126/science.1174921

Zhang, X.M., B. Walsh, C.A. Mitchell, and T. Rowe. 2005. TBC domain family, member 15 is a novel mammalian Rab GTPase-activating protein with substrate preference for Rab7. *Biochem. Biophys. Res. Commun.* 335:154–161. doi:10.1016/j.bbrc.2005.07.070